Assessing pluvial flood hazard potential using multi-criteria decision making and iterative ensemble smoothing in New York City, Long Island, and Long Island Sound watersheds

Robert J. Welk*[1] (0000-0003-0852-5584), Kalle Jahn[1] (0000-0002-4976-0137), Liv Herdman[1] (0000-0002-5444-6441), Robin Glas[1] (0000-0002-7394-1667), Kristina Masterson[1] (0000-0001-7717-0751), Salme Cook[1] (0000-0003-1129-6209)

[1] U.S. Geological Survey, New York Water Science Center, Troy, New York, USA
*Corresponding author: rwelk@usgs.gov,
2045 NY-112 Coram New York, Building 4
(631) 736-0783

Highlights

- We developed a spatially distributed metric for assessing pluvial flood hazard that relies on publicly available data.
- We piloted the addition of parameter optimization to multi-criteria decision making to evaluate assessment accuracy.
- We identified key driving factors contributing to rainfall accumulation.
- The approach is easily adaptable to accommodate various spatial scales (meters and above).

Abstract

Exposure to pluvial floods poses significant hazards, and predicting flood locations can be challenging. We developed a metric that quantifies relative flood hazard across Long Island, New York and the watersheds surrounding Long Island Sound. Based on surface topography, land surface characteristics, and historical weather patterns, we identified seven factors with readily available data that can contribute to rainfall accumulation. Using publicly available spatial datasets, we employed a Multi-Criteria Decision Making (MCDM) framework to generate spatially distributed hazard ranks based on initial assumptions regarding the drivers of pluvial flooding in the study area. To mitigate some subjective biases inherent in the MCDM framework, we employed Iterative Ensemble Smoothing (iES), which allowed for variation in input parameters and aligned model outputs with a target dataset of observed flood events, resulting in a more quantitative analysis. The comparison of MCDM with and without iES demonstrated improved performance with the incorporation of iES estimated parameters. The methods allow for weighting of driving factors of flood hazard. Future studies could explore obtaining observed flood event records that are more consistently spatially distributed across the study area and consider how existing stormwater infrastructure may be mitigating current pluvial flood hazard potential.

Keywords

Pluvial flooding, GIS, iterative ensemble smoothing, hazard assessment, multi-criteria-decision-making

1.Introduction

Pluvial flooding, commonly referred to as flash flooding, occurs due to intense rainfall events. These floods arise when the rainfall rate exceeds the infiltration capacity of underlying soils and overwhelms natural and manmade drainage systems. Flood occurrence is influenced by land cover, subsurface properties, and atmospheric conditions. Pluvial floods pose significant hazards to human health and infrastructure, and may lead to casualties (Ashley and Ashley, 2008) and extensive damage to property and public utilities (Ahmadalipour and Moradkhani, 2019). The spatial extent of impacts, typically manifesting within six hours of rainfall initiation, is challenging to forecast due to the sudden onset of storms and the detailed knowledge required about topography, drainage systems, and other infrastructure for predicting locations of water accumulation. Identifying areas prone to pluvial flooding is crucial for effective management and decision-making, enabling targeted resource allocation to support flood risk management and enhance resilience in high-flood hazard zones.

The work presented here focuses on developing a pluvial flood hazard metric for the City of New York (hereafter, New York City), Long Island, and Long Island Sound watersheds in Westchester County, southern Connecticut, and southwestern Rhode Island (Figure 1). This area includes a wide range of population density, land use, topography, and soil characteristics (Figure 2). Land cover acquired from the National Land Cover Dataset (U.S. Geological Survey, 2019) ranges from largely developed (>70% in all New York City Boroughs and Nassau County) to mostly forested in New London and Middlesex Counties in Connecticut. Agriculture is not prevalent in the more developed areas but makes up 6.6% of land area in eastern Suffolk County on Long Island. Due to the highly developed landcover in major urban centers and surrounding suburbs, impervious surface is common; within New York County (Manhattan), approximately 76% of the landcover is categorized as impervious. There is some variation in rainfall patterns with more annual precipitation on average in the northern, higher elevation parts of the study area in Connecticut, but more intense events are more common in Nassau and Suffolk Counties (Figure 3). Pluvial flood hazards pose a significant threat to this region, particularly due to the extensive developed land cover and exposure to tropical storm tracks, which often result in high-intensity rainfall events (Agel et al., 2015).

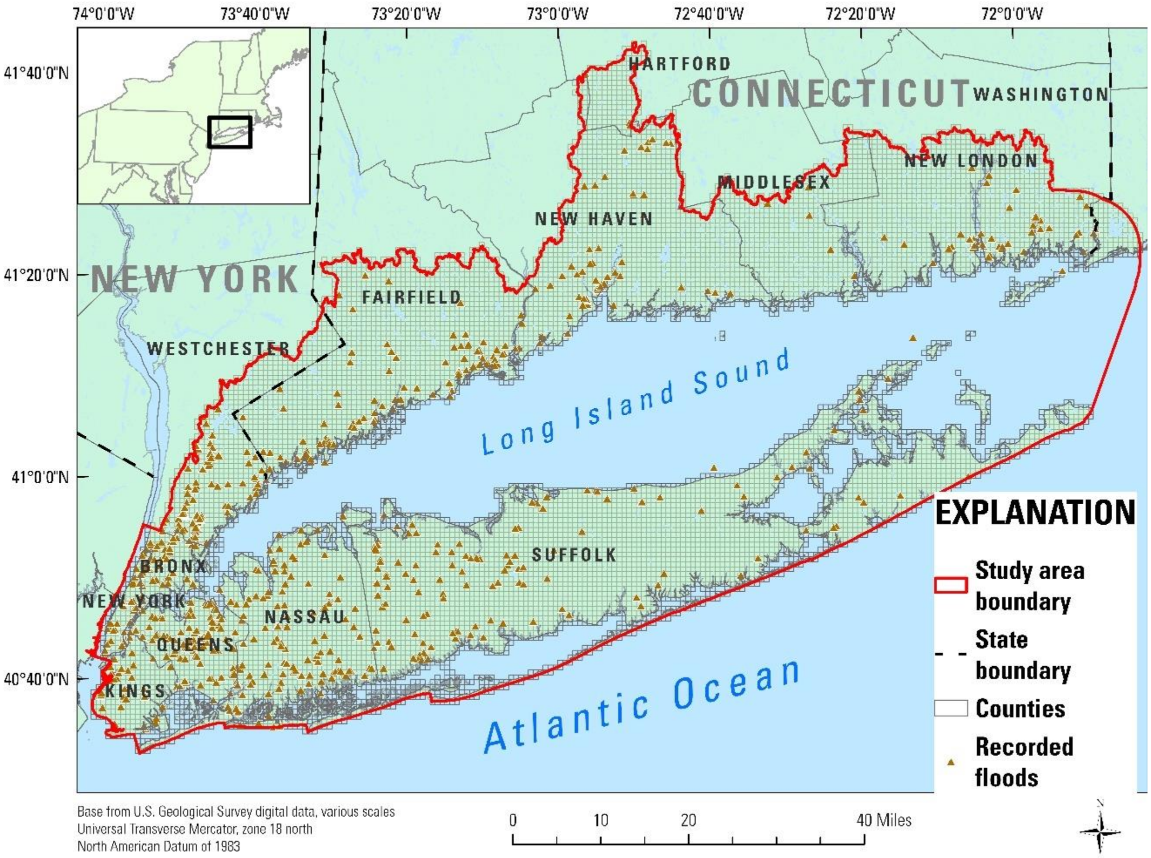

Base from U.S. Geological Survey digital data, various scales
Universal Transverse Mercator, zone 18 north
North American Datum of 1983

Figure 1. Map of study area with model polygrid cells and recorded floods from National Oceanic and Atmospheric Administration (NOAA) Storm Events Database (2021).

Flash floods in New York and Connecticut have severe impacts on both urban and rural areas, exacerbating existing infrastructure vulnerabilities and posing substantial flood hazard potentials to public safety and property. In urban centers such as New York City, NY and New Haven, CT, sudden and intense rainfall can overwhelm drainage systems, leading to street inundation and basement flooding, which disrupt daily activities and transportation networks and threaten public health. The associated economic losses from property damage, business interruptions, and emergency response operations are substantial. In more rural regions flash floods threaten residential communities and agricultural lands, often causing erosion, crop damage, and compromised water quality in local water bodies (Vozinaki et al., 2015).

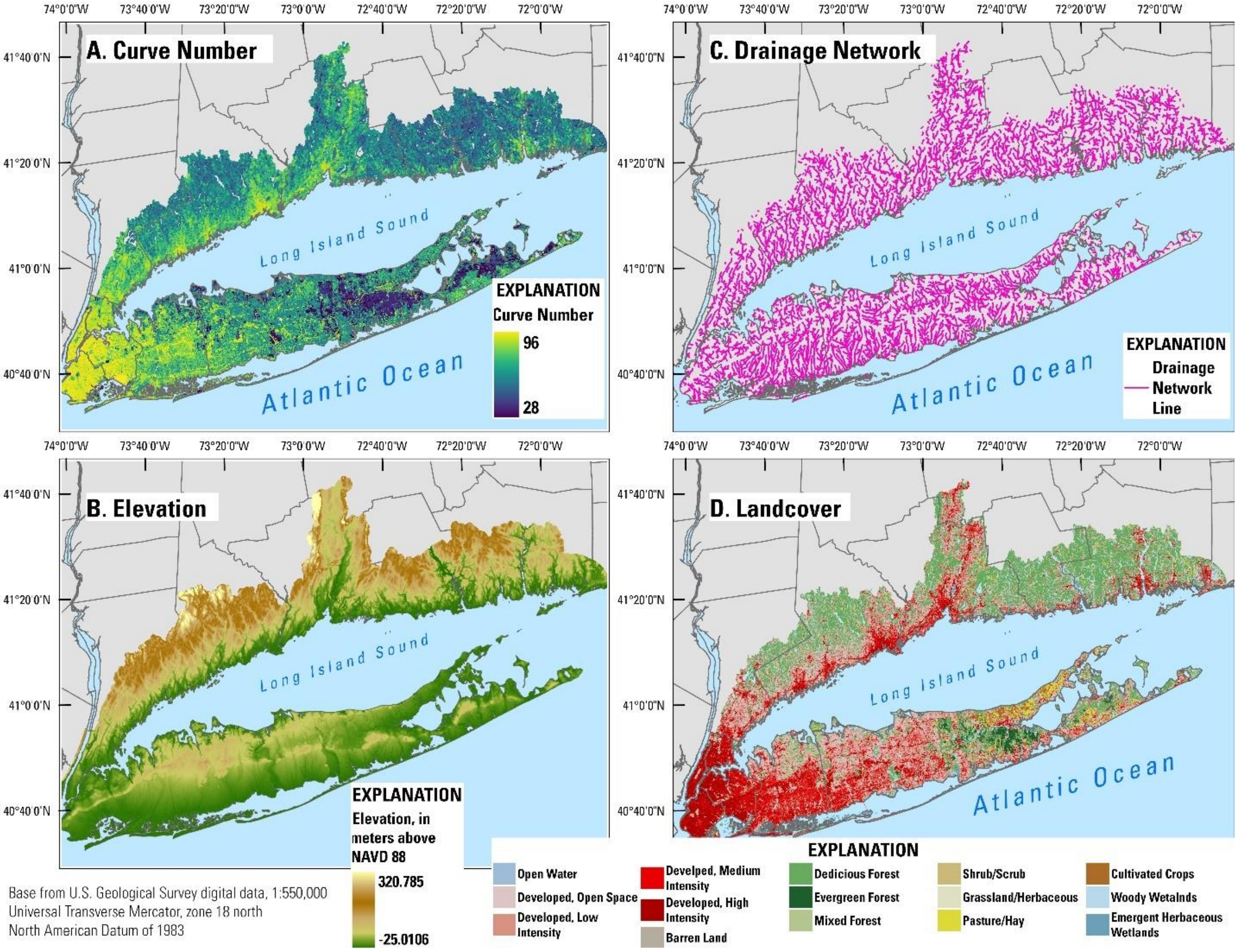

Base from U.S. Geological Survey digital data, 1:550,000
Universal Transverse Mercator, zone 18 north
North American Datum of 1983

Figure 2. Map showing distributions of input factors across study area. (A) Curve number from Finkelstein (2022) and Holland and Barclay (2024) soil-water-balance models. (B) Land surface elevation in feet above the North American Vertical Datum of 1988 (NAVD88) from U.S. Geological Survey 1/3 Arc Second Digital Elevation Model (2020). (C) Polylines representing drainage network derived from U.S. Geological Survey 1/3 Arc Second Digital Elevation Model (2020). (D) National Land Cover Dataset landcover categories from U.S. Geological Survey National Landcover Dataset (2019).

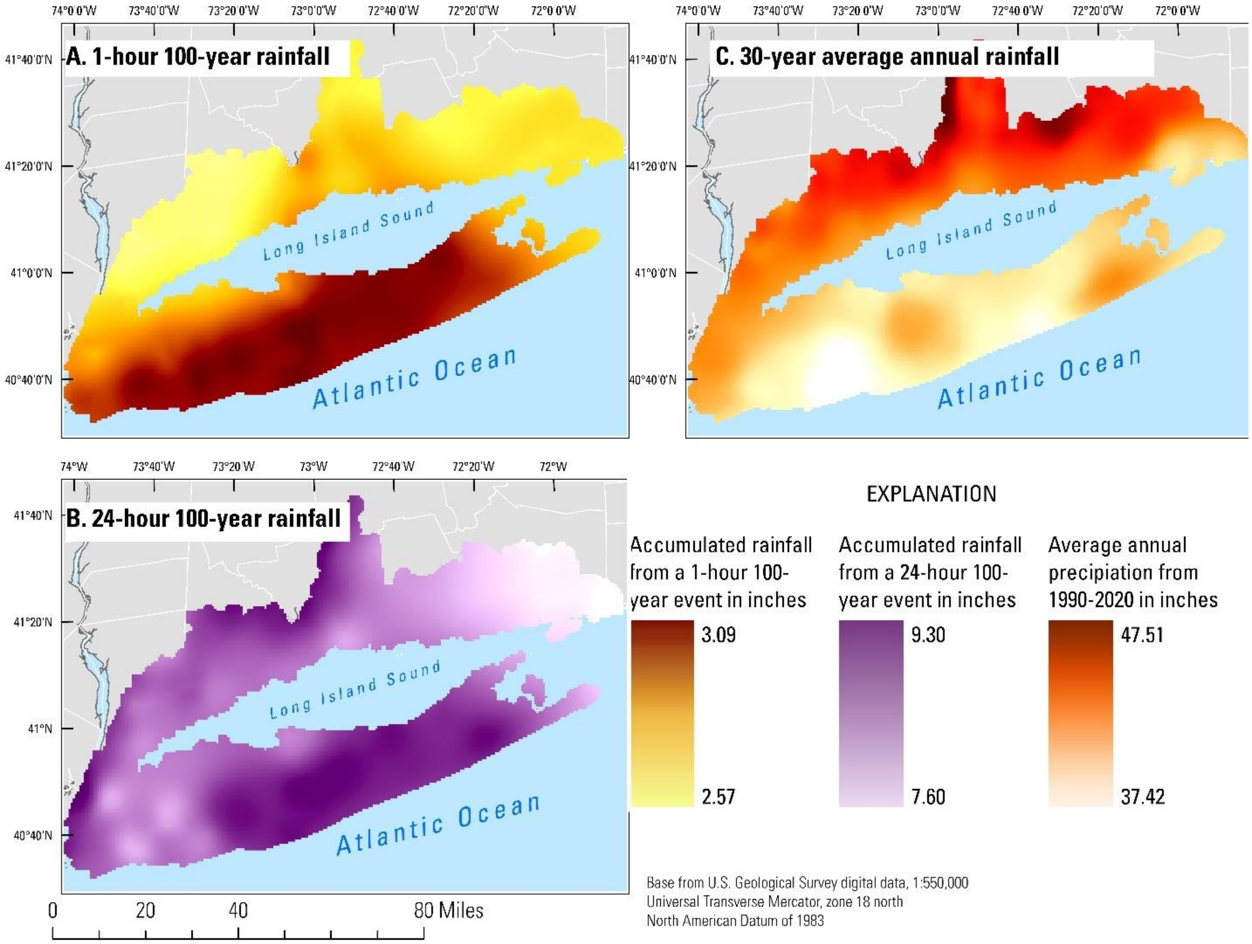

Figure 3. Map showing distributions of precipitation input factors. (A) Accumulated rainfall in inches for a 1-hour 100-year rainfall event from National Oceanic and Atmospheric Administration (NOAA) Atlas 14 (2019). (B) Accumulated rainfall for a 24-hour 100-year rainfall event from NOAA Atlas 14 (2019). (C) Average annual precipitation in inches for years 1991-2020 from PRISM Group 30-Year Normals (2022).

Communities within the study area have experienced significant damage caused by numerous storms in recent years. In August 2014, a rapid onset storm in Long Island brought over 13 inches of rain to the Town of Islip, NY in just a few hours, causing major flooding on roadways and stranded vehicles. The drainage systems were designed to sustain a 5-inch storm over a 24-hour period, which was insufficient to manage the heavy rainfall. The excessive precipitation also caused sinkholes to form, septic tanks to collapse, and basements to flood (Caina et al., 2021). In September 2021, the remnants of Hurricane Ida struck the region as an extratropical cyclone, bringing extreme rainfall and resulting in 43 deaths in New York, Connecticut, New Jersey, and Pennsylvania. Most of the fatalities were due to drownings that occurred in basement apartments in Boroughs of Brooklyn and Queens due to 6 inches of rain falling in a few hours (Marnin, 2021). During July 2023 in New Haven and Fairfield Counties in Connecticut and in New York, severe weather events resulted in substantial damage to both residential and agricultural areas (Goode, 2023). These events are several examples that highlight the vulnerability of the study area to flash floods and the need for effective mitigation strategies at targeted locations.

Studies conducted across the five Boroughs of New York City, Long Island, and southern Connecticut have shown varying influences on the severity of pluvial flooding. Aging drainage infrastructure, poor natural drainage, and low-lying areas have been associated with pluvial flood events in New York City (Rosenzweig et al., 2018). Additionally, pluvial flooding in New York City has been shown to be exacerbated by extreme precipitation, drainage backups, and clogged catch basins (Agonafir et al., 2022). New York City has performed several studies and developed mitigation strategies like Cloudburst Hubs, the blue belt program, and green infrastructure to mitigate pluvial flood risk (New York City Department of Environmental Protection, n.d). The New York City sewer system is only designed for 0.6 to 1.5 inches per hour rainfall rates, and several recent hurricanes superseded those rates and led to loss of lives and property (Ghanbari et al., 2024). The high prevalence of studies of pluvial flood hazard in New York City have given way to several informative hazard and risk maps, but these maps do not extend beyond city lines.

Beyond New York City, across Long Island and the shorelines of Long Island Sound, studies of pluvial flood risk have shown broadly that exposure to tropical and extratropical cyclone tracks coupled with varying degrees of surface runoff potential are the strongest predictors of pluvial flooding (Coch, 2015). For the southern Connecticut River Basin, which includes several coastal counties, urban pluvial flooding was best predicted by proximity to water bodies and elevation, whereas rural pluvial flooding was better predicted with surficial materials that may impede or facilitate infiltration (Giovannettone et al., 2018). Over the past half century, the development of impervious surfaces has increased while the urban-agricultural gradient of Long Island from west to east has been maintained. Additionally, near-surface water tables have been getting higher. These changes are impeding natural drainage and have increased runoff over the past half century (Glas et al., 2023). Across Long Island, subsurface drainage networks have substantially altered the runoff dynamics (Jefferson et al., 2017; Locatelli et al., 2017); however, accessing digital information describing the drainage infrastructure is challenging because it depends on the capabilities of individual cities or counties to digitize and share this information with the public (Shrestha et al., 2022).

In addition to the regional studies, there are some nationally available products to assess exposure to flood hazards in the study area. These include floodplain mapping and Flood Insurance Rate Maps from Federal Emergency Management Agency (FEMA) (Federal Emergency Management Agency , n.d.), alerts and warnings from the National Weather Service (NWS) (National Weather Service, n.d.), and The National Water Model developed by the National Oceanic and Atmospheric Administration (NOAA, n.d.), a hydrologic modeling framework that simulates observed and forecast streamflow over the entire continental United States (National Oceanic and Atmospheric Administration, n.d.). Both New York and Connecticut use geographic information system (GIS) mapping platforms that incorporate data from national sources and other flood hazard potential information like land use, and infrastructure to visualize flood hazards such as the NYC Flood Hazard Mapper (NYC Department of City Planning, n.d.). In addition, local governments and organizations develop their own community-focused tools and resources that focus on flood hazard potential assessment and emergency management. The current suite of tools and resources, however, is generally focused on other causes of flooding, such as elevated coastal water levels and overflowing river channels but does not contain evaluation of flood hazard potential from flash flooding at a regional scale.

This study introduces a framework for a regional-scale assessment of pluvial flood hazard potential using Multi-Criteria Decision Making (MCDM) integrated with GIS and Iterative Ensemble Smoothing (iES). MCDM is a systematic approach that incorporates multiple factors influencing outcomes by considering stakeholder perspectives. MCDM has been applied across various fields, including business, healthcare, engineering, public policy, and environmental studies (Sahoo and Goswami, 2023). In hydrologic studies, MCDM has been used for evaluating flood management, land use planning, water resource management, community engagement, and climate change adaptation (Yilmaz and Harmancioglu, 2010; Ngubane et al, 2024; Geng and Wardlaw, 2013; Karymbalis et al., 2021; Abdullah et al., 2021). In this study, MCDM is applied to flood hazard assessment to integrate factors influencing pluvial flooding and identify high-flood hazard potential zones guiding targeted mitigation and adaptation measures at regional and subregional scales. The Analytic Hierarchy Process (AHP), introduced by Saaty (1980), is a widely used MCDM technique that evaluates qualitative and quantitative factors through pairwise comparisons. This study employs AHP to evaluate seven factors influencing pluvial flood onset and assess flood hazard potential over a region.

Previous research developed a methodology for integrating AHP with GIS for flood hazard assessment (Karymbalis et al., 2021); however, determining the relative importance of factors affecting pluvial flooding has been reliant on assumptions regarding the relationship between flood influencing factors and flood onset. This study complements the AHP framework with iterative ensemble smoothing (iES) to optimize factor weights based on observed flood events by integrating model-independent parameter estimation and uncertainty analysis using PEST++ software (version 5.0; White et al., 2020). This calibration aligns factor weighting with observed flash flood occurrences, producing a spatially distributed metric, henceforth referred to as hazard rank, that quantifies the hazard potential of pluvial flooding in the watersheds surrounding Long Island Sound (Figure 1).

This paper describes the development of the pluvial hazard rank for Long Island Sound. In section 2, the publicly available input data and processing methods are described. In section 3, the methods used for both the AHP and iES are discussed. Section 4 assesses the model and shares results of the pluvial hazard rank. Section 5 discusses the results and highlights the shortcomings of this process and suggests the next logical extensions of the work; finally, the paper is concluded in Section 6.

2. Data and data processing

The methods employed in this study used publicly available spatial datasets as inputs, which were processed using GIS (ArcGIS Pro, Esri, Redlands, CA). To harmonize datasets of differing resolutions, the study area was subdivided into 11,407 grid cells, each 900-meter by 900-meter (approximately 3,000-feet by 3,000-feet) (Figure 1). This standard grid was also used for calculation and mapping of the grid to accommodate harmonization of multiple spatial data sets of different resolutions. We opted to select a grid size aligned with the coarsest of our data sets to minimize the impact of any downscaling. Multiple spatial layers that were identified as drivers of potential flood hazard were aggregated to the grid. To map the spatial distribution of pluvial flood hazard potential and identify pluvial flood drivers over the region, weights of flood-influencing factors were calculated using AHP and parameter optimization. Seven factors were identified as potentially contributing to pluvial flood onsets and aggregated to the grid - curve number, drainage network density, topographic slope, ponding fraction, 30-year average rainfall, and 1-hr and 24-hour 100-year return period rainfall accumulation (Figure 3, 4).

The curve number rainfall-runoff relation is based on basin properties of soil type, land use, surface cover, and antecedent runoff condition and has been shown to have strong influence in pluvial flood prediction (Wang et al., 2019). Curve numbers typically range from 30 to 100, with higher values representing greater surface runoff potential. These higher curve numbers describe the general inability of the surface to absorb precipitation, which can lead to overland water accumulation (Cronshey et al., 1986). Curve numbers were calculated from land cover and soil properties using the methods described in Westenbroek et al. (2010).

Two factors, drainage density and slope, were derived from a National Elevation Dataset 1/3 arc-second (~10-m) resolution Digital Elevation Model (DEM; U.S. Geological Survey, 2020). Drainage density quantifies the abundance of drainage networks over a defined geographic region, indicating areas where runoff accumulation may occur based on topographic characteristics. The sum of the lengths of drainage networks (3rd order and greater) in each grid was divided by the land area of the grid to get the drainage density. The drainage density gives an estimate of the hydrologic properties of the surface and subsurface – high densities indicate areas where water preferentially flows overland rather than infiltrating to the subsurface. Slope refers to the steepness or degree of incline of a surface based on topographic relationships and was calculated from the DEM using standard GIS geoprocessing tools (Calculate Slope ArcGIS Pro).

The ponding fraction is the total area of closed depressions within a grid cell divided by the total land area of the grid and indicates where runoff is expected to accumulate under extreme rainfall conditions. Closed depressions are defined as a landform where the elevation is lower than the surrounding elevation and were calculated from a 1-meter lidar-derived DEM using methods described by Doctor and Young (2013) and Sporleder et al. (2021). Closed depression prevalence can be indicative of flood hazard potential in both urban and rural settings (Liu et al., 2023) because accumulated runoff can exceed storage capacity resulting in flooding in surrounding areas. All known recharge basins and other features with geometries resembling recharge basins and other large stormwater infrastructure were removed from the areas designated as closed depressions, following the methodology of Sporleder et al. (2021).

Rainfall variability was addressed using average precipitation and 100-year events of 1-hour and 24-hour duration (Figure 3). The gridded 30-year normal precipitation product from Oregon State University (PRISM Group, 2022) for years 1991–2020 was used to calculate the average annual precipitation for a grid cell. This metric is used to designate areas that generally have wetter antecedent conditions. To estimate the likelihood of extreme rainfall events, NOAA intensity duration curves were used (National Oceanic and Atmospheric Administration, 2019) (Figure 3). The rainfall accumulation from a storm with a 100-year return period and 1-hour duration and the rainfall accumulation from a storm with a 100-year return period and 24-hour duration quantify rainfall amounts from short-duration and long-duration extreme events, respectively.

A dataset of points representing recorded flash flood events from 2006-2020 was assembled from the NOAA National Centers for Environmental Information Storm Events Database (NOAA, n.d.) (Figure 1) and was filtered to obtain only records associated with flash floods. The set of records was used to calibrate the weights of flood influencing factors for the iES with AHP approach. Grid cells with one recorded flood were given a hazard rank target of 3 (moderate flood hazard potential). Grids with two recorded floods were assigned a hazard rank target of 4 (high flood hazard potential). Grids with three or more recorded floods were given a hazard rank target of 5 (very high flood hazard potential). Of the 11,407 grid cells in the study area, 507 grids were targeted to be a flood hazard rank of 3, 88 had a flood hazard rank of 4, and 38 had a flood hazard rank of 5.

3. Methods

MCDM is a process used to evaluate and prioritize criteria in complex situations where a single criterion cannot be used. In this application of MCDM, weights are applied to each criterion to identify flood hazards. Coefficient weights were determined using either AHP or iES with AHP as the starting point, as described below. The coefficient weights of each variable were multiplied by the binned factor grid values to obtain a parameter flood hazard potential score per factor for each grid cell. The seven variable flood hazard potential scores were summed and normalized to a scale of 1 to 5 to obtain spatially distributed relative flood hazard potential ranks for the study area.

3.1. Analytic Hierarchy Process

The methodology described in Karymbalis et al. (2021) for integrating AHP and GIS was followed with some modifications. Similar to their methodology, an expert group provided an informed estimate of pairwise relative importance (Welk et al., 2025) which was used to create weighting coefficients for each of the seven flood influencing factors. To apply these weighting coefficients, we first discretized each of the factors by binning observations into five groups with approximately equal numbers of members and assigned a label (1-5) in order of increasing flood hazard exposure potential as specified in Table 1 and shown in Figure 4. Other binning choices were investigated, and the uniform binning was found to result in better matching of observations. Specifically, the experts were asked to identify the relative numeric importance for flood risk for each factor when compared pairwise to every other factor (21 total comparisons). The comparisons were assembled into a 7-by-7 matrix [Table 2]. For example, in cell 1,2 (highlighted), curve number is given importance 7 relative to closed depression area (ponding percentage), 3. The use of relative numeric assessments requires that the diagonal of the table is all 1s because no factor can be more or less important than itself, and the lower left part of the table is the reciprocal of the upper right. This expert-assigned relative importance matrix was then used to determine factor coefficient weights for each input by performing a series of linear algebra calculations (Saaty, 1980) resulting in a set of factor weights for the seven flood influencing factors [Table 1]. The coefficient weights of each variable were then multiplied by the binned factor grid values to obtain a parameter flood hazard potential score per factor for each grid cell. The seven variable flood hazard potential scores were summed and scaled from 1 to 5 to obtain spatially distributed relative flood hazard potential ranks for the study area. This calculation of hazard with the expert assigned weights is referred to as the AHP estimate.

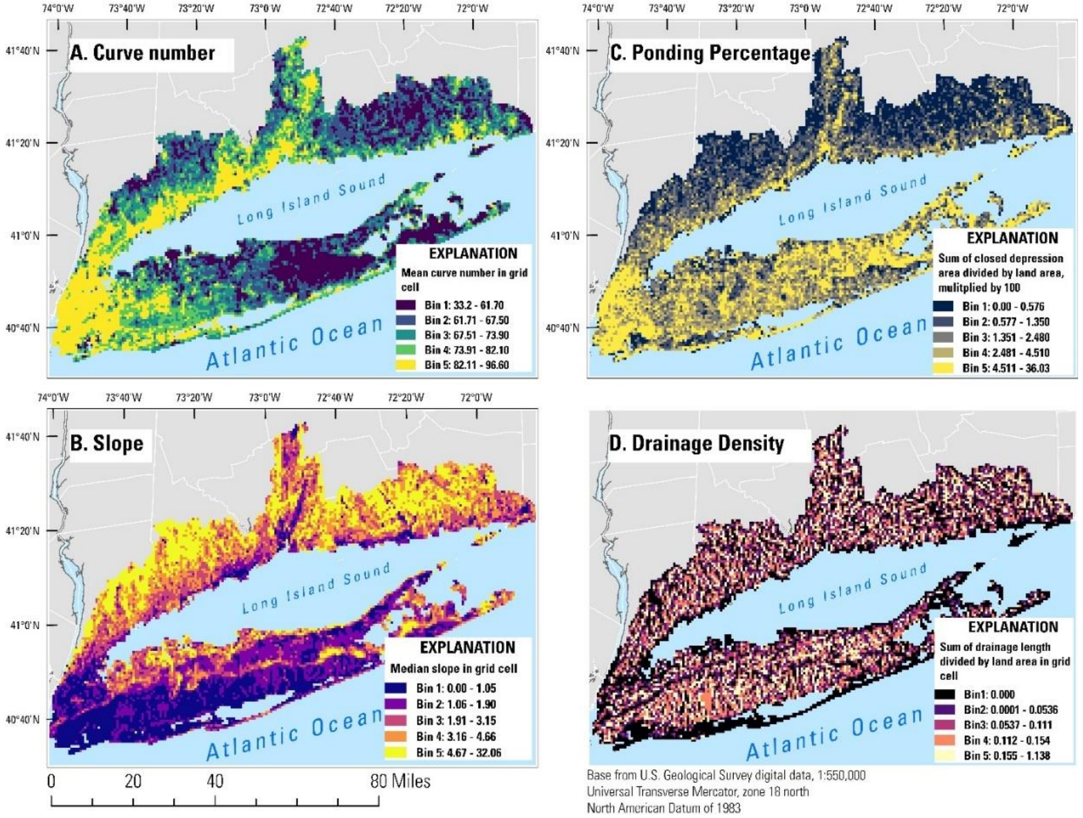

Base from U.S. Geological Survey digital data, 1:550,000
Universal Transverse Mercator, zone 18 north
North American Datum of 1983

Figure 4. Flood influencing factors aggregated to a 900-meter by 900-meter polygrid. (A) Curve number derived from Finkelstein (2022) and Holland and Barclay (2024) soil-water-balance models. (B) Slope derived from U.S. Geological Survey 1/3 Arc Second Digital Elevation Model (2020). (C) Ponding Percentage derived from U.S. Geological Survey Coastal National Elevation Database (2017) and U.S. Geological Survey Coastal and Marine Geology Sandy LiDAR (Woolpert, 2014). (D) Drainage Density derived from U.S. Geological Survey 1/3 Arc Second Digital Elevation Model (2020).

Table 1. Polygrid aggregation functions, with binned label assignments shown in parentheses as the range of factor values associated with each bin. Final weights are calculated using the Analytic Hierarchy Process (AHP), both with and without the inclusion of iES, for each of the seven flood-influencing factors. Data source: Welk (2025).

Factor Name	Aggregate Function	Binned Label Assignments 1	2	3	4	5	AHP Coefficient Weight	AHP with iES Coefficient Weight
Slope	**Median**	**[0, 1.05]**	**(1.05, 1.9]**	**(1.9, 3.15]**	**(3.15, 4.66]**	**(4.66, 32.06]**	**2**	**1**
Curve Number	**Mean**	**[33.2, 61.7]**	**(61.7, 67.5]**	**(67.5, 73.9]**	**(73.9, 82.1]**	**(82.1, 96.6]**	**7**	**8.4**
Closed Depression	**Sum**	**[0, 0.576]**	**(0.576, 1.350]**	**(1.35, 2.480]**	**(2.480, 4.510]**	**(4.51, 36.03]**	**3**	**3.4**
Drainage Density	**Sum**	**[0]**	**[0.0001, 0.0536]**	**(0.0536, 0.111]**	**(0.111, 0.154]**	**(0.154, 1.14]**	**3**	**2.0**
30-Year Rainfall	**Mean**	**[37.42, 39.69]**	**(39.69, 40.54]**	**(40.54, 41.76]**	**(41.76, 43.15]**	**(43.15, 47.45]**	**2.6**	**1.3**
1-Hour Rainfall	**Mean**	**[2.58 , 2.68]**	**(2.68, 2.79]**	**(2.79, 2.89]**	**(2.89, 2.99]**	**(2.99, 3.09]**	**2.6**	**2.5**
24-Hour Rainfall	**Mean**	**[7.60, 8.14]**	**(8.14, 8.30]**	**(8.30, 8.47]**	**(8.47, 8.69]**	**(8.69, 9.29]**	**2.6**	**1.6**

Table 2. Analytic Hierarchy Process (AHP) pairwise comparison matrix defining the relative importance of seven flood-influencing factors: Curve Number, Ponding Percentage, Slope, Drainage Density, and rainfall metrics (1-hour, 24-hour, and long-term rainfall). Data source: Welk (2025).

	Curve Number	**Ponding Percentage**	**Slope**	**Drainage Density**	**1-Hour Rain**	**24-Hour Rain**	**Long-term Rain**
Curve Number	**1**	**7/3**	**7/2**	**7/3**	**14/5**	**14/5**	**14/5**
Ponding Percentage	**3/7**	**1**	**3/2**	**1**	**6/5**	**6/5**	**6/5**
Slope	**2/7**	**2/3**	**1**	**2/3**	**4/5**	**4/5**	**4/5**
Drainage Density	**3/7**	**1**	**3/2**	**1**	**6/5**	**6/5**	**6/5**
1-Hour Rain	**5/14**	**5/6**	**5/4**	**5/6**	**1**	**1**	**1**
24-Hour Rain	**5/14**	**5/6**	**5/4**	**5/6**	**1**	**1**	**1**
Long-term Rain	**5/14**	**5/6**	**5/4**	**5/6**	**1**	**1**	**1**

3.2. Iterative ensemble smoothing

The expert weights identified through the AHP methodology were refined using the iterative ensemble smoothing (iES) algorithm within PEST++ (White et al., 2020). Specifically, the iES algorithm adjusted the weights to better fit the target hazard values, potentially mitigating biases from the expert-derived relative ranks calculated from AHP alone. The iES technique builds on a Monte Carlo approach by evaluating an ensemble of potential parameter values, resulting in an observation residual vector and weighted objective function for each member of the parameter ensemble. From this information, the iES algorithm calculates an updated ensemble of parameter values to evaluate. Several updated iterations are performed, with each iteration yielding an ensemble of objective function values and further constraining the distribution sampled to generate the parameter ensemble. In this application, the coefficient weights for flood influencing factors were allowed to vary, enabling a better match to the target hazard values for each grid cell. These target hazard values were established based on observations of recorded flood events, with the frequency of such events in each grid cell determining the corresponding hazard level, as previously described.

The relative importances assigned to the seven flood influencing factors were treated as parameters, and best-fit values were estimated using iES in PEST++ (White et al., 2020). The relative importance values identified by the expert panel through AHP were used as the initial values for the iES analysis (refer to Table 1). An initial ensemble was generated by stochastically sampling normal distributions centered around these initial parameter values, with absolute lower and upper bounds set at 1.0 and 9.0, respectively. These bounds were chosen because there is an inherent reciprocal relationship of weights when creating the pairwise matrix, and allowing values outside of this range implies more certainty than can be justified with this process. Additionally, sampling with normal distributions is standard practice in line with the assumption that expert starting values are more likely. However, this sampling strategy does not preclude significant changes from the AHP estimate weights to the iES determined weights. This process produced 500 realizations, forming the ensemble for the iES upgrading process.

The objective function was defined with the hazard level targets from observed flood events with a goal of producing a simulated hazard level equal to or greater than the observed target level, meaning that a simulated value exceeding a target was considered a good fit, whereas a simulated value below the target was deemed a poor fit. To represent validation target uncertainty, an ensemble of target realizations was generated by stochastically sampling normal distributions centered on each target and standard deviations set-based target value: target 3s were assigned a standard deviation of 0.25, target 4s and 5s were assigned a standard deviation of 0.5. Setting a minimum threshold for targets, as opposed to the exact value, was done to mitigate bias from fewer reported flood events, and the larger standard deviations for the higher targets represent higher uncertainty for those values. Where no flood events were observed, there was no impact on the objective function, thus not limiting locations with no reported floods to be constrained to low flood risk. Functionally, this target "noise" allowed us to evaluate if the iES ensembles would be able to encompass the target ensembles prior to running parameter upgrades to understand how the parameter upgrade process might be skewed by outlier targets while also providing more flexibility for iES to match targets (i.e., wider target distributions reduce extreme parameter adjustments to match targets compared to narrower target distributions). To better understand the effect of this target uncertainty, iES runs were also performed without "noise" which resulted in functionally identical results as the runs with target uncertainty.

The initial parameter ensemble was used in a Monte Carlo analysis to determine if the means of any simulated equivalents in the ensemble were more than 4 standard deviations from its corresponding mean in the target plus noise ensemble. Targets that fell outside this statistical distance were labeled in "prior data conflict" (White et al, 2020), meaning that iES would be unable to match them through parameter upgrades, and they were thus dropped during iES to avoid skewing the upgrade process. Parameter realizations were excluded during the iterative process if they resulted in a consistency ratio greater than 0.2, ensuring the logical soundness of the pairwise comparisons (Saaty, 1980). iES also includes a "base" realization, a specific ensemble member that starts with the initial expert values and does not incorporate uncertainty in the observed values during parameter upgrades between iterations. The base can be used as a representative realization when a single realization is required for further analyses.

Using a spatially distributed set of flood hazard potential ranks derived from the iES estimate, a hot-spot analysis was conducted to evaluate the spatial variability of pluvial flood hazard potential by identifying areas where high flood hazard potential scores are clustered. The analysis involved calculating the Getis-Ord Gi* test statistic, which is a measure of spatial autocorrelation. This method quantifies the similarity of values among neighboring features in relation to the entire study area for each grid cell. The Getis-Ord Gi* statistic yields a z-score and corresponding p-value for each grid cell, indicating whether the spatial association of that cell with its neighbors differs significantly from what would be anticipated under the null hypothesis of spatial randomness (Ord and Getis, 1995). High positive z-scores, denoting "hot spots," signify clusters of high ranks surrounded by other high values, thereby clarifying areas of concentration. A significance level of 0.10 was employed as the threshold for hot-spot classification.

4. Results

4.1. Model Assessment

The use of iES improved the model assessment of hazard ranks compared to the targets. Figure 5 illustrates the distribution of target values based on the initial parameters assigned by experts, alongside the distribution of the final targets simulated final iES base realization. The iES objective function value, Phi, showed the most substantial reduction during the first two iterations, with minimal changes observed in the third iteration. Consequently, the second iteration was chosen as the iES ensemble.

In the base realization, which represents the parameter set that best matches observations without uncertainty, the iES weights better matched simulated values to all three target groups (3, 4, and 5) than the initial expert weights (Figure 5), as anticipated given the reductions in Phi. For target group 3, the median and quartiles increased from 3.42 and 3.04/3.80 in the AHP estimate to 3.56 and 3.12/3.96 in the iES. Similarly, for target group 4, the median and quartiles increased from 3.6 and 3.23/3.87 in the AHP estimate to 3.78 and 3.44/4.09 in the iES. For target group 5, the median and quartiles increased from 3.79 and 3.37/4.01 in the AHP estimate to 3.98 and 3.63/4.21 in the iES. Although the largest change was in target group 5, the median of iES simulated values (3.98) remained below the target of 5, with only two simulated values reaching or exceeding 4.5. For target group 4, the number of simulations that reached the target threshold increased from 22 (AHP) to 34 (iES). Mean absolute error (MAE) decreased in target groups 4 and 5 when using iES weights compared to AHP: from 0.52 to 0.47 for group 4, and from 1.21 to 1.07 for group 5. In contrast, MAE increased slightly in group 3, from 0.65 to 0.74.

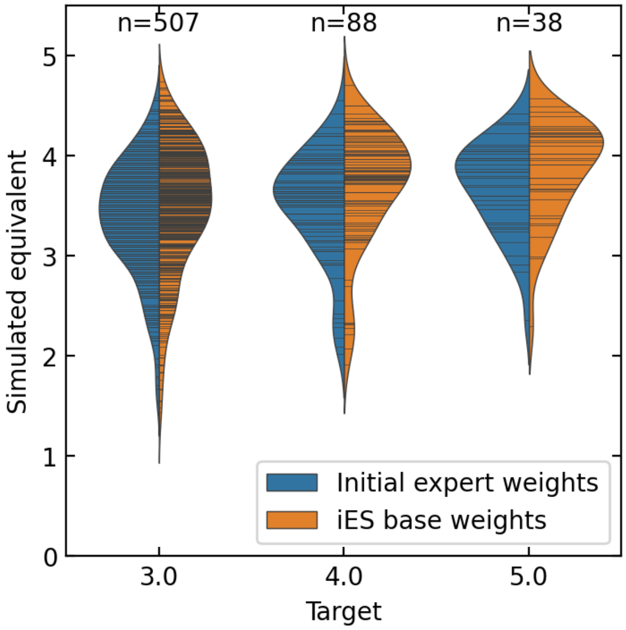

Figure 5. Distributions of target matching for the AHP estimate and iES base weight realizations. Each horizontal black line within a distribution represents a target.

Six targets were dropped from iES because they were in prior data conflict, and some patterns were observed. As described in 3.2, these targets were removed because their inclusion would have resulted in a skewed iES objective function. Four of the six are in New London, Connecticut, one is in the central north shore of Long Island, New York, and one is in the Borough of Bronx, New York. The New London targets and the Long Island target are located near groups of high residual model cells in the final iES ensemble, which could be due to errors in the target data within those specific areas, nuanced processes within those areas that are not captured by model inputs, or a combination of both. The conflict target in Borough of Bronx, however, is surrounded by simulated values matching the greater-than condition for their respective targets and may be a function of differences in scale between the model grid cell size and the point location observations that are accounted for in the targets.

Although the magnitudes of the weights changed during iES, the overall pattern expected by the experts was confirmed by iES. Except for the closed depression and 1-hour rainfall intensity factors, the iES base factor weights were adjusted by at least one weight unit from the initial base factor weights (Figure 6). Curve number was weighted nearly 1.5 units higher in the iES relative to the initial and remained substantially higher than all the other factors because it had been placed in the AHP estimate. Slope was given the least weight in the iES ensemble (nearly all realizations had slope with a weight of 1), followed by the 24-hour rainfall intensity and 30-year normal rainfall. Most of the relative importances selected for the prior bore out in the iES. The magnitude of the weights shifted, with curve number and closed depressions having their relative importance increased while slope, drainage density, 24-hour rainfall intensity, and the 30-year normal rainfall, received lower weights. The weight of the one-hour rainfall intensity did not change significantly between initial and iES. The relative importance of the rainfall factors showed a decreasing trend with increasing duration, with the 1-hour rainfall intensity weighted higher than the 24-hour rainfall intensity, which was weighted higher than the 30-year normal rainfall.

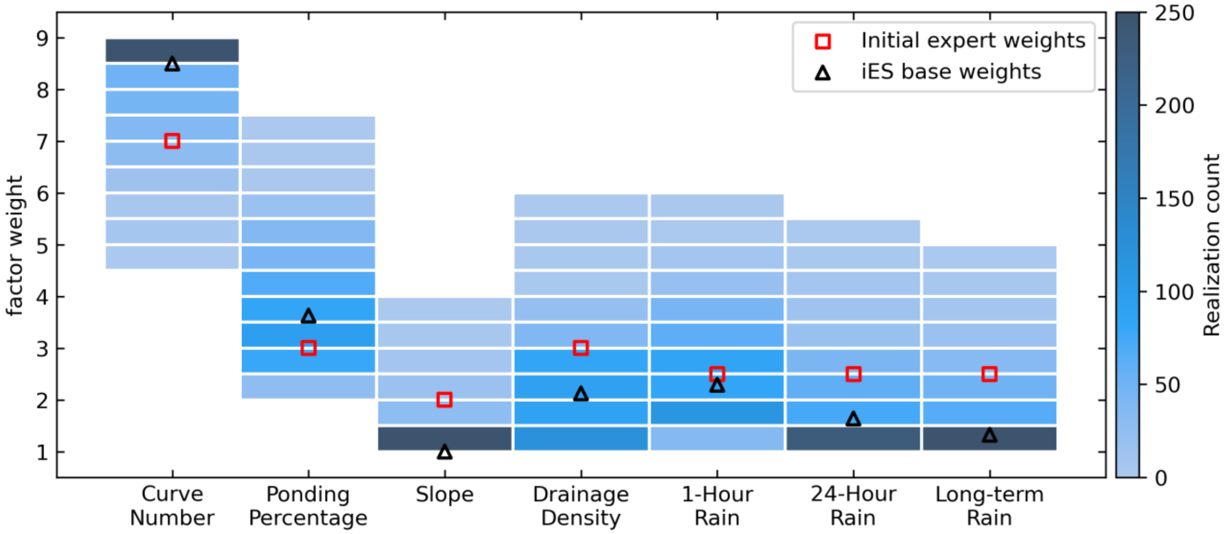

Figure 6. Distribution heatmaps of factor weights for the iES realization ensemble (n=464). Distributions are binned in 0.5 weight increments, with darker color indicating higher realization count (refer to colorbar). Open red squares show the expert assigned base weight for each factor, and open black triangles show the iES base weight for each factor.

4.2. Total hazard rank

The total hazard ranks were computed using the optimal weights determined from iES. The optimized factor weights (black triangles in Figure 6) derived from the selected iES realization were applied to weight the ranked (binned) factors for each grid cell, and these values were subsequently summed. The resulting sums were rescaled on a scale of 1 to 5, representing low to high flood hazard potential, and can be interpreted as the relative flood hazard from pluvial flooding across the study area. The results of the hazard ranks from both the AHP estimate and iES model weights are shown in Figure 7 (Panel A and B) and as a shapefile in Welk et al. (2025).

The model exhibited a general inability to classify grid cells as high flood hazard potential (hazard ranks greater than 4) throughout the entire domain (Figure 5). Under-prediction in the AHP estimate hazard rank was particularly prevalent in grid cells characterized by low levels of urbanization, while targets achieving a score of three were more successfully matched (refer to Supplement Figure S1). The overall spatial pattern of higher hazard ranks in urban areas does not change significantly from the AHP estimate rank to the iES generated estimates (Figure 7). This indicates that the model does not significantly deviate from the fundamental understanding of rainfall hazard by experts. However, when examining the differences between the iES estimate and the AHP estimate ranks (Figure 7 Panel C), the iES generated ranks are generally higher in more urbanized areas (such as New York City, Westchester, and Nassau Counties) and lower in the less developed regions of the study area due to the increased weight attributed to curve number in the iES estimate relative to the AHP estimate. Inherent in the math of the final ranks, it is rare to obtain a hazard rank of 5 with a curve number below the 80th percentile. When we examine the factors of the cells in our study area that receive a hazard rank over 4.5, we find that the curve number and ponding percentage were both above the 80th percentile as was slope. Although mathematically possible to get a hazard rank of 5 with a low slope, perhaps due to some spatial structure in the dataset, we do not observe this in the Long Island region. Due to the importance of curve number and ponding percentage in the overall rank, it is not surprising that those values are higher than average in the highly ranked cells. The counties with the highest average hazard ranks were Kings (Borough of Brooklyn), New York (Borough of Manhattan), Bronx, and Queens Counties with ranks of 4.18, 4.17, 3.86 and 3.86, respectively. The counties with the lowest average ranks were Middlesex, New London, and Washington Counties with ranks of 2.08, 2.16, and 2.28, respectively.

The centroids of grid cells exceeding 0.10 significance level in the Getis-Ord Gi* test statistic were subsequently plotted as a kernel density map, as illustrated in Figure 7, panel D. This method identified dense hot spot regions that are coincident with areas of higher population density (including NYC, southern Nassau County, and New Haven County). The highest relative exposure to flood hazards typically occurs in densely populated urban centers, with particularly pronounced clusters identified in the Boroughs of New York City. Additionally, hot spots are observed in western Long Island, southern central Long Island, the south fork of eastern Long Island and northern New Haven County and southern Hartford County in Connecticut along the Connecticut River.

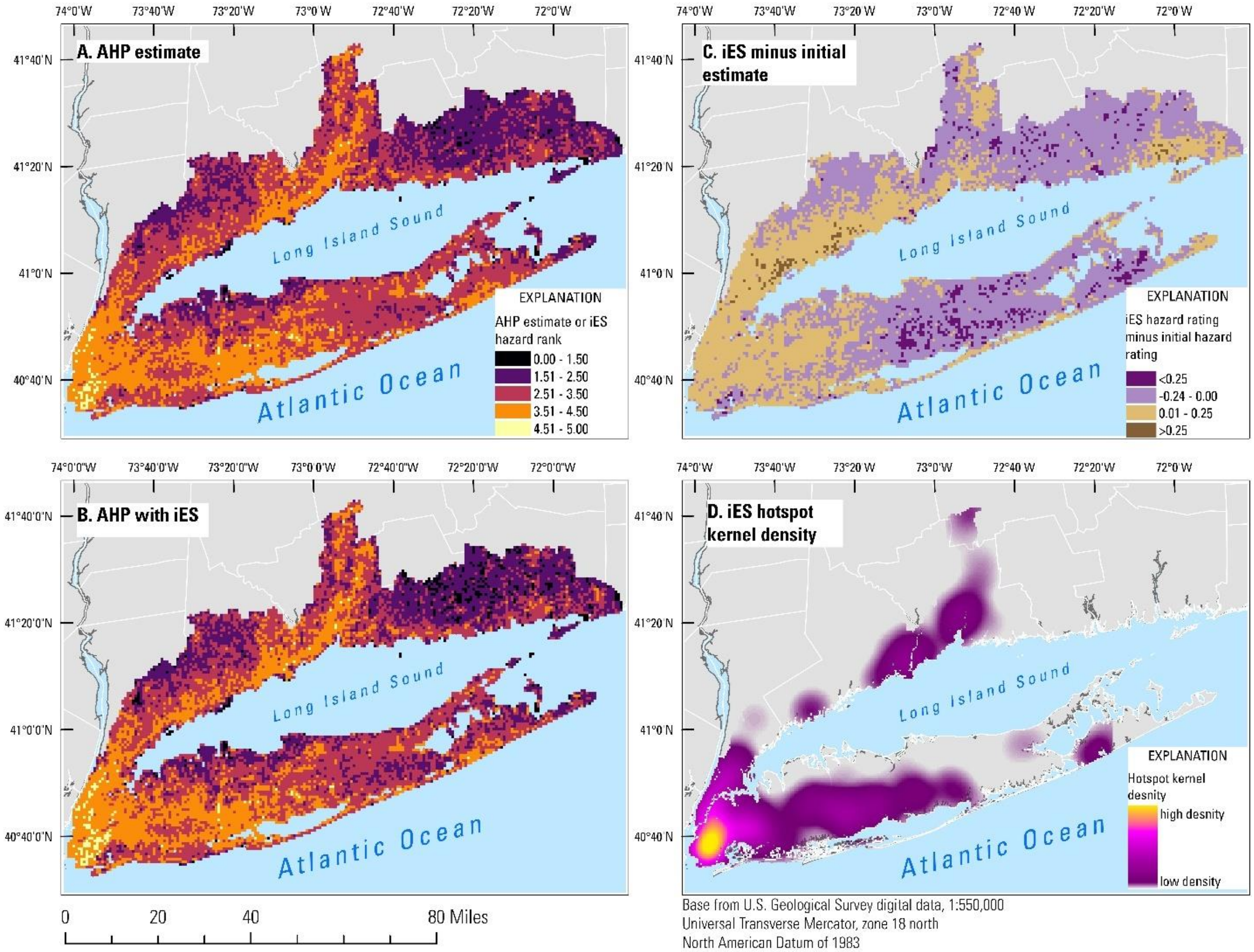

Base from U.S. Geological Survey digital data, 1:550,000
Universal Transverse Mercator, zone 18 north
North American Datum of 1983

Figure 7. Maps of MCDM results derived from Welk, 2025. **(**A**)** AHP-estimated hazard ranks. **(**B**)** iES hazard ranks.**(**C**)** Difference between AHP-estimated and iES hazard ranks. **(**D**)** Kernel density mapping of cells with 0.10 significance in the Getis-Ord Gi* hotspot test.

There are no clear spatial patterns in under- or over-prediction of the flood hazard rank. During the iterative ensemble smoothing process, an allowance for over-prediction (flood hazard potential scores exceeding target values) was made, meaning that only under-prediction was classified as an error. Figure S1 in the Supplement shows the spatial distribution of residuals in the iES estimate (hazard rank minus target) for the cells that had at least one recorded flood event. An analysis of the scores revealed that the top 20% (n = 309) correlated with at least one recorded flood event. Similarly, an almost equivalent number (n = 324) of the bottom 80% scores also contained at least one flood observation. Furthermore, among the top half of scores, 519 were associated with flood events, whereas only 114 in the bottom half had recorded flood events. It can be inferred from analysis of the residuals that the observation of flood events is not evenly geographically distributed. There is a much higher density of observations in New York City and the western end of Long Island.

5. Discussion

The methods presented in this study expand on previous flood hazard analyses (Karymbalis et al., 2021) that incorporate Multi-Criteria Decision Making (MCDM) into spatial mapping by providing a quantitative framework that weights inputs to match hazard with observed pluvial flooding. By integrating the Iterative Ensemble Smoothing (iES) framework to optimize model outputs with recorded flood events, we have reduced some of the subjectivity commonly associated with MCDM applications. This methodology highlights the challenges of quantitatively assigning ranks within MCDM. While the AHP estimates effectively captured the order of importance of each factor, iES adjusted the relative strengths of these factors.

A significant limitation of the methodology employed arises from the flood event data used as hazard rank targets. The NOAA Storm Events Database compiles flood events from various sources, leading to potential inconsistencies in observation accuracy (Teale and Winter, 2024). Additionally, flood event databases tend to be biased toward heavily populated areas, where such events are more likely to be reported. As a result, factor weights may disproportionately favor variables correlated with population density, such as curve number, which exhibited a significantly higher weight in the iES estimate compared to other inputs. Furthermore, assigning targets based on the number of flood events in a grid cell is itself a subjective decision that was driven (in part) by the type and amount of data that were available for assessing hazard. Additionally, reporting thresholds for events are not defined and so are not inherently consistent across the study area. Also, the need to analyze these factors requires the assignment of an event to a particular grid cell; however, each flood event may have a spatial extent that extends into a neighboring grid cell. Although the “greater than” restriction for target assignment mitigates the importance of assignments, there remain relatively few targets to match ranks greater than 4. While the objective function set to be greater than the assigned target is designed to minimize the impact of missing observations, the potential bias of more observations in higher population areas would impact our results. The final map of hazard would demonstrate a focus on floods that have tangible human/ economic consequences. Thus, the flood map is likely calibrated toward events that are more relevant to decision making and management.

Although we filtered the storm database to only capture flood events reported to be caused by high rainfall, the conditions experienced prior to and during individual flood observations vary widely; some events are associated with exceptionally high rainfall, while others occur with relatively low precipitation. However, accurately associating rainfall amounts with the observed flood events across the study area is difficult due to the low density of observation in the study area. In particular, the atmospheric mechanisms that generate intense summer thunderstorms are relatively small in horizontal extent, and this prevents us from estimating the rainfall in each grid cell based upon a rainfall station more than a few kilometers away (Miller and Frederick 1969). Because most of the flood events selected from the database were observed in June, July, August and September, the small spatial extent of storms during events is even more likely. Thus, it is difficult to develop rigorous time varying criterion for flooding, and we are forced to utilize static input criteria.

Interesting patterns are observed when we examine in more detail how the contributing factors contribute to the overall hazard ranks. The distributions of curve number and ponding percentage (Figure 8a, b, respectively) are shown in relation to the target ranks. Similar plots for other factors are provided in the Supplement in Figure S2a-e. The average ponding percentage increases slightly with increasing target value, although the highest ponding percentages are assigned a target of 3 or greater. Conversely, curve number exhibits a lower average value for the highest validation targets. However, the model we used to predict hazard ranks requires a linear dependence on each of these factors; thus, the higher curve number values lead to greater hazard ranks. As a result, when examining the distribution of the input factors with each validation target (Figure 8a, b), there is an increase in the average value; however, there can be significant deviations from this mean for any of the given criteria, which highlights the interactive nature of these different variables. For example, ponded water on a surface with low curve number may not cause significant flooding because the ponded water could infiltrate through the surface down to the groundwater. The model is not able to capture this interaction, but this interaction would impact our calibration targets and make it difficult to clearly separate the dependence on a given factor. This interaction is one example of why the most important contributing factors could not be differentiated to create a strong distinction between the characteristics associated with ranks of 4 or 5. Because the range of driving factors does not differ in the target data, the model extrapolates the relationship between 3 and 4 to produce the range of targets from 4 to 5. The development of a more sophisticated model that allows nonlinear dependence and or interaction between the factors might ameliorate the issue, but a more complex model runs the risk of overfitting and thus losing its potential for more general applicability. Alternatively, additional input factors may be needed to predict the highest hazard rank and differentiate between scores of 4 and 5.

(a) Curve Number

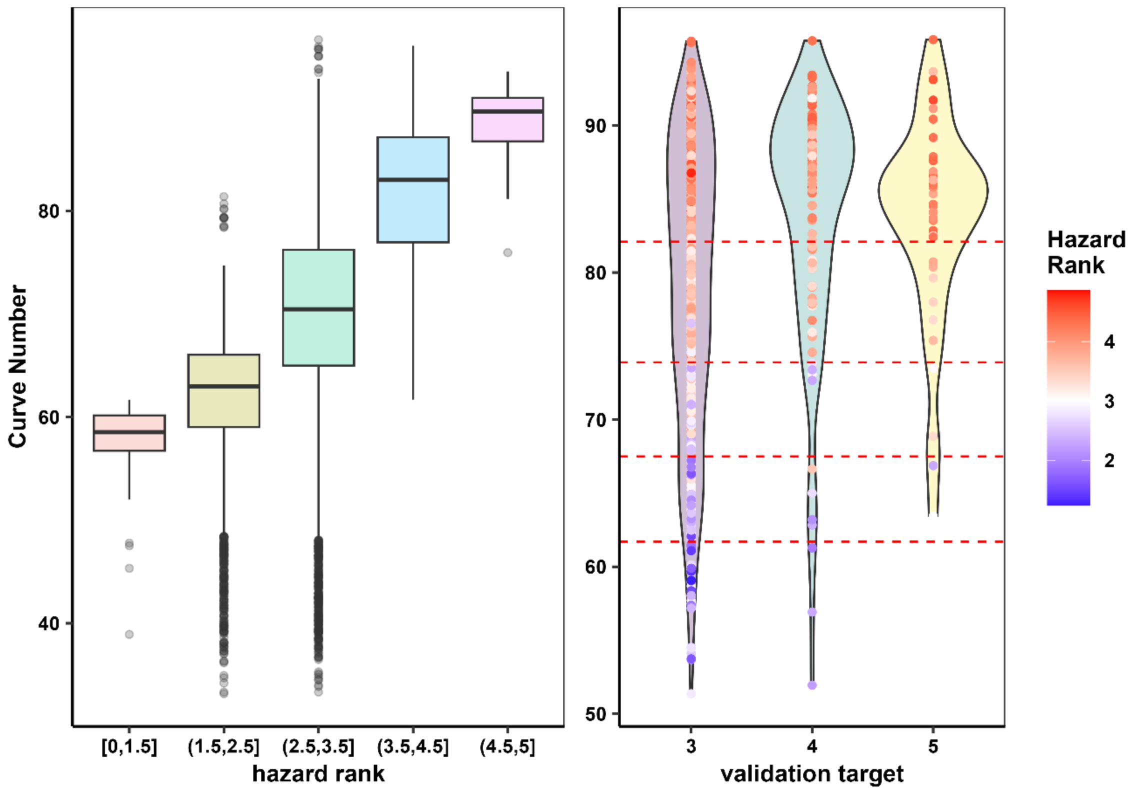

(b) Ponding Percentage

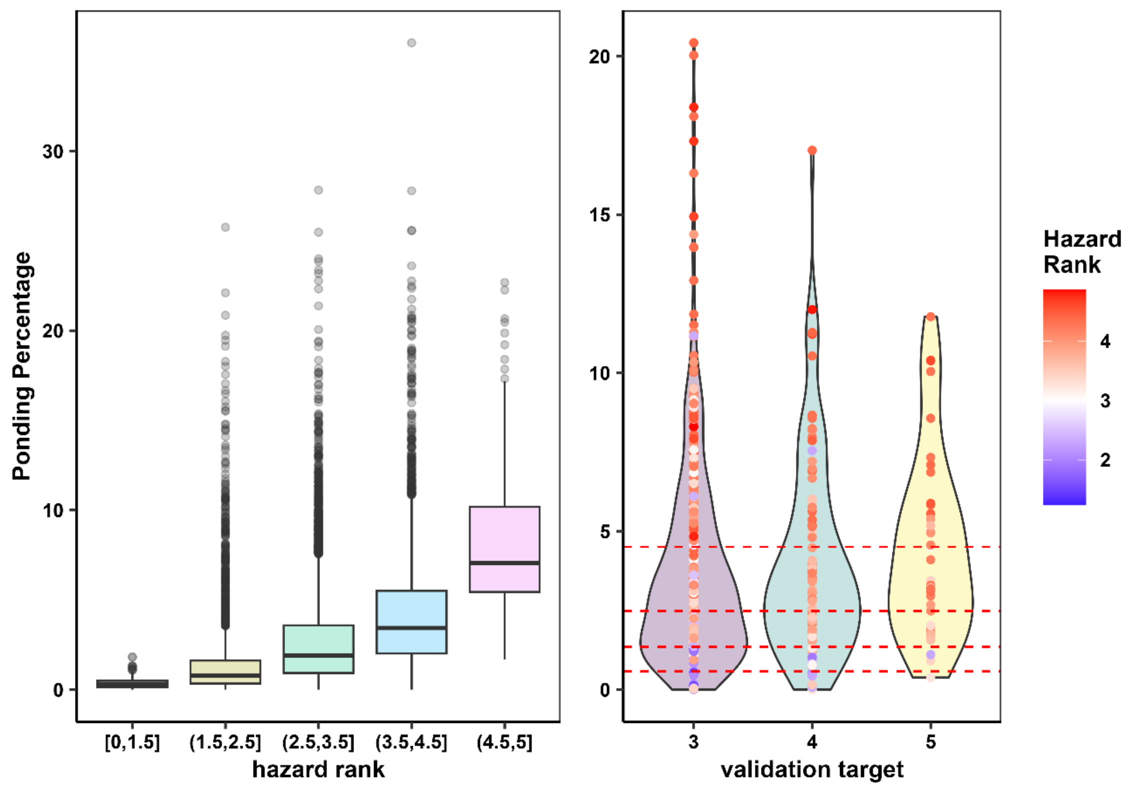

Figure 8a-b. [redacted] Distributions of flood influencing factors binned by hazard rank (left) and validation target group (right). Each row corresponds to a different factor: (a) curve number, (b) ponding percentage. For each row, the left panel shows a boxplot of factor distributions grouped by binned hazard ranks and the right panel shows factor distributions binned by target group, with points representing iES hazard rank. Red dotted lines indicate bin divisions.

Another limitation of the MCDM approach is the initial assignment of relative factor importance and the binning of factors into discrete categories (1-5 label assignments). Different iterations of binning into categories were attempted: one with natural breaks and another using the standard deviations from fitting a normal distribution. Neither approach resulted in lower MAE values in the final iES ensemble relative to the target values, indicating that these binning strategies did not improve model performance. For some flood-influencing factors, the relationship with flood hazard potential remains ambiguous. For instance, we assumed that closed depression density would lead to increased flooding due to runoff accumulation. However, these features may also indicate areas where stormwater management infrastructure is more likely to be integrated, potentially mitigating flood hazard risks. Although the methods used to generate the ponding areas (Sporleder et al. 2021) do some filtering to remove larger manmade drainage features, these methods would not be able to detect the presence of smaller infrastructure such as a storm sewer drain. A comparative analysis which considered both scenarios (depressions worsening or alleviating flood potential), indicated that the initial assumption better aligned with the target dataset. However, it is possible that the wider distributions of ponding percentage (Figure 8b) are consistent with this ambiguous relationship and not only due to interactions with land surface type or other variables as discussed earlier. Nevertheless, the geographic distribution and effectiveness of stormwater infrastructure in flood management remains a large uncertainty in this model, underscoring the need for generalized assumptions regarding contributing factors, despite inherent variations.

The methods presented in this study omit consideration of the mitigating effects of stormwater infrastructure for several reasons. Data on the effectiveness and location of contributing areas for such infrastructure are often of inconsistent quality and coverage within the study area. Some infrastructure may be under-designed or poorly maintained, resulting in suboptimal performance. In extreme events, when runoff volume exceeds the system's design capacity, existing infrastructure can exacerbate flood conditions (Wang and Gourbesville, 2023). Therefore, this study focuses on evaluating the vulnerability of the study area to flash floods without accounting for the mitigating effects of stormwater infrastructure. A logical next step would be to expand our analysis to include additional inputs, such as stormwater capacities; however, digital information of this type is not available for all areas of the study domain currently.

In an ideal situation, we would sufficient data to provide a quantified level of hazard related to pluvial flooding. In this work, hazard target events were the best available dataset of pluvial flooding hazard. Currently, substantially more data are available on the location and occurrence of coastal and riverine floods. The USGS collects high water marks for various storms (USGS Flood Event Viewer, n.d.); however, these flood events are often from hurricanes or other events with compounding influences, and thus the hazard associated with rainfall cannot be identified. Collection of additional data on location, flooded area, and flooded depth during rainfall events could improve our ability to model rainfall hazard.

6. Conclusion

The methodologies developed in this research can help advance pluvial flood hazard assessment by providing a flexible and practical approach that can be adapted to various contexts. This study has established a framework for assessing pluvial flood hazard potential at a regional scale, but this framework can be implemented at various scales to accommodate the available resolution of input data that influence exposure to flood hazards. By integrating Multi-Criteria Decision Making (MCDM) with Geographic Information Systems (GIS) and Iterative Ensemble Smoothing (iES), we have developed a methodology that identifies high-risk areas and uses continuous, nationally accessible datasets as inputs. This broad applicability could help communities facing similar challenges assess flood hazards across diverse geographic regions. The simplicity of the GIS/MCDM calculations enhances the general adaptability of this methodology and could help stakeholders and managers easily interpret and apply the findings.

Furthermore, while existing tools have primarily focused on coastal and riverine flooding, this study fills an information gap by performing a regional pluvial flood hazard assessment. The spatial representation of areas with elevated flood hazard potential, along with the contributing factors, can be a resource in regional planning and emergency management frameworks. By identifying areas with high flood hazard potential, decision-makers can allocate resources more effectively and implement proactive measures to safeguard public safety and property. By highlighting the input factors that are driving the hazard, a manager can identify what mitigations might be effective. Continued refinement of these methodologies, along with the integration of real-time data and community input, could help enhance the accuracy and relevance of pluvial flood risk assessments.

Authors' contribution

Robert Welk: Conceptualization, Data Curation, Methodology, Formal analysis, Writing - original draft, Visualization

Kalle Jahn: Conceptualization, Formal analysis, Methodology, validation, visualization, Writing - original draft

Liv Herdman: Conceptualization, Formal analysis, Funding Acquisition, Methodology, Project administration, Writing - original draft

Robin Glas: Conceptualization, Methodology, Writing - original draft

Kristina Masterson: Investigation, Funding acquisition, Writing - original draft, Project administration, Supervision

Funding

Funding to support this study was provided by the Environmental Protection Agency as part of the Sustainable and Resilient Communities goal of the Long Island Sound Study.

Declaration of Competing Interest

The authors declare that they have no known competing financial interests or personal relationships that could have appeared to influence the work reported in this paper.

Data availability

Geospatial Datasets of Pluvial Flood Influencing Factors Used to Assess Compound Flood Exposure Potential in Coastal New York and Connecticut - ScienceBase-Catalog

Welk, R., Glas, R., Herdman, L., and Fisher, B. (2025). Geospatial datasets of pluvial flood influencing factors used to assess compound flood exposure potential in coastal New York and Connecticut: *U.S. Geological Survey Data Release*. https://doi.org/10.5066/P9N6J1SN.

References

Abdullah, M., Siraj, S., and Hodgett, R. (2021) An Overview of Multi-Criteria Decision Analysis (MCDA) Application in Managing Water-Related Disaster Events: Analyzing 20 Years of Literature for Flood and Drought Events. *Water*; 13(10), 1358. https://doi.org/10.3390/w13101358

Agel, L., Barlow, M., Qian, J., Colby, F., Douglas, E., and Eichler, T. (2015). Climatology of Daily Precipitation and Extreme Precipitation Events in the Northeast United States. *Journal of Hydrometeorology*, *16*(6), 2537-2557. https://doi.org/10.1175/JHM-D-14-0147.1

Agonafir, C., Pabon, A., Lakhankar, T., Khanbilvardi, R., and Devineni, N. (2022). Understanding New York City street flooding through 311 complaints. *Journal of Hydrology*, *605*, 127300. https://doi.org/10.1016/j.jhydrol.2021.127300

Ahmadalipour, A. and Moradkhani, H. (2019). A data-driven analysis of flash flood hazard, fatalities, and damages over the CONUS during 1996–2017. *Journal of Hydrology*, 578. https://doi.org/10.1016/j.jhydrol.2019.124106

Ashley, S. and Ashley,W. (2008). Flood Fatalities in the United States. Journal of *Applied Meteorology and Climatology*, 47, 805–818. https://doi.org/10.1175/2007JAMC1611.1

Caina, C, Porter, D, and Peltz, J. (2021). More than 45 dead after Ida's remnants blindside Northeast. Associated Press. https://apnews.com/article/northeast-us-new-york-new-jersey-weather-60327279197e14b9d17632ea0818f51c

Coch, N. (2015). Unique Vulnerability of the New York–New Jersey Metropolitan Area to Hurricane Destruction. *Journal of Coastal Research,* 31 (1): 196–212. https://doi.org/10.2112/JCOASTRES-D-13-00183.1

Cronshey, R., McCuen, R., Miller, N., Rawls, W., Robbins, S., and Woodward, D. (1986). Urban Hydrology for Small Watersheds (2nd Edition). U.S. Department of Agriculture, Soil Conservation Service, Engineering Division, Technical Release 55.

Doctor, D. and Young, A. (2013). An evaluation of automated GIS tools for delineating karst sinkholes and closed depressions from 1-meter LiDAR-derived digital elevation data NCKRI Symposium 2: Proceedings of the Thirteenth Multidisciplinary Conference on Sinkholes and the Engineering and Environmental Impacts of Karst. *KIP Talks and Conferences*, 26. https://digitalcommons.usf.edu/kip_talks/26

Federal Emergency Management Agency. (n.d.). Flood Maps. https://www.fema.gov/flood-maps

Finkelstein, J.S. (2022). Soil-water-balance model archive for Long Island, NY, 1900-2019: U.S. Geological Survey data release, https://doi.org/10.5066/P94OLK6Z.

Geng, G. and Wardlaw, R. (2013). Application of Multi-Criterion Decision Making Analysis to Integrated Water Resources Management. *Springer Nature*, 27, 3191–3207. https://doi.org/10.1007/s11269-013-0343-y

Ghanbari, M., Dell, T., Saleh, F., Chen, Z., Cherrier, J., Colle, B., and Arabi, M. (2024). Compounding effects of changing sea level and rainfall regimes on pluvial flooding in New York City. *Natural Hazards*, *120* (7), 6377-6400. https://doi.org/10.1007/s11069-024-06466-8

Giovannettone, J., Copenhaver, T., Burns, M., and Choquette, S. (2018). A statistical approach to mapping flood susceptibility in the Lower Connecticut River Valley Region. *Water Resources Research*, *54*(10), 7603-7618. https://doi.org/10.1029/2018WR023018

Glas, R., Hecht, J., Simonson, A., Gazoorian, C., and Schubert, C. (2023). Adjusting design floods for urbanization across groundwater-dominated watersheds of Long Island, NY. *Journal of Hydrology*, *618*, 129194. https://doi.org/10.1016/j.jhydrol.2023.129194

Goode, S. (2023). Farmers in CT devastated by rain and flooding. *CT Insider*. https://www.ctinsider.com/connecticut/article/wethersfield-microburst-storm-ct-flood-farms-18204340.php

Holland, M.J., and Barclay, J.R. (2024). Soil-Water-Balance model developed to simulate net infiltration in watersheds on the north shore of the Long Island Sound: U.S. Geological Survey data release, https://doi.org/10.5066/P1GUC7FE

Jefferson, A. J., Bhaskar, A. S., Hopkins, K. G., Fanelli, R., Avellaneda, P. M., and McMillan, S. K. (2017). Stormwater management network effectiveness and implications for urban watershed function: A critical review. *Hydrological Processes*, *31*(23), 4056-4080. https://doi.org/10.1002/hyp.11347

Karymbalis, E., Andreou, M., Batzakis, D.-V., Tsanakas, K., and Karalis, S. (2021). Integration of GIS-Based Multicriteria Decision Analysis and Analytic Hierarchy Process for Flood-Hazard Assessment in the Megalo Rema River Catchment (East Attica, Greece). *Sustainability*, 13(18), 10232. https://doi.org/10.3390/su131810232

Liu, W., Zhang X., Feng Q., Yu, T., Engel, B. (2023). Analyzing the impacts of topographic factors and land cover characteristics on waterlogging events in urban functional zones. *Science of The Total Environment*, 904. https://doi.org/10.1016/j.scitotenv.2023.166669

Locatelli, L., Mark, O., Mikkelsen, P. S., Arnbjerg-Nielsen, K., Deletic, A., Roldin, M., and Binning, P. J. (2017). Hydrologic impact of urbanization with extensive stormwater infiltration. *Journal of Hydrology*, *544*, 524-537. https://doi.org/10.1016/j.jhydrol.2016.11.030

Marnin, J. (2021). Ida's Remnants Prompt Weather Service to Issue First-Ever Flash Flood Warnings in NY. *Newsweek*. https://www.newsweek.com/idas-remnants-prompt-weather-service-issue-first-ever-flash-flood-warnings-ny-1625419

Miller, J.F. and Frederick, R.H. (1969). The precipitation regime of Long Island, New York. United States Department of the Interior, Geological Survey. https://doi.org/10.3133/pp627A

National Oceanic and Atmospheric Administration (2021). *Storm Events Database* [Data set]. National Centers for Environmental Information. https://www.ncdc.noaa.gov/stormevents/

National Oceanic and Atmospheric Administration (2019). NOAA Atlas 14: Precipitation-Frequency Atlas of the United States. Volume 10. https://hdsc.nws.noaa.gov/pfds/

National Oceanic and Atmospheric Administration. (n.d.). National Water Model, U.S. Climate Resilience Toolkit. https://toolkit.climate.gov/tool/national-water-model

National Weather Service (n.d.). NWS Alerts. https://alerts.weather.gov/search

Ngubane, Z., Bergion, V., Dzwairo, B., Stenström, T. A., and Sokolova, E. (2024). Multi-criteria decision analysis framework for engaging stakeholders in river pollution risk management. *Scientific reports*, 14(1), 7125. https://doi.org/10.1038/s41598-024-57739-y

NYC Department of City Planning. (n.d.). NYC Flood Hazard Mapper, https://dcp.maps.arcgis.com/apps/webappviewer/index.html?id=1c37d271fba14163bbb520517153d6d5

New York City Department of Environmental Protection. (n.d.). Flood prevention. https://www.nyc.gov/site/dep/environment/flood-prevention.page

Ord, J.K. and Getis, A. (1995). Local Spatial Autocorrelation Statistics: Distributional Issues and an Application. *Geographical Analysis*, 27: 286-306. https://doi.org/10.1111/j.1538-4632.1995.tb00912

PRISM Group (2022). PRISM 30-Year Normals. Oregon State University. https://prism.oregonstate.edu, https://www.prism.oregonstate.edu/normals/

Rosenzweig, B. R., McPhillips, L., Chang, H., Cheng, C., Welty, C., Matsler, M., and Davidson, C. I. (2018). Pluvial flood risk and opportunities for resilience. *Wiley Interdisciplinary Reviews: Water*, *5*(6). https://doi.org/10.1002/wat2.1302

Saaty, T. L. (1980). The Analytic Hierarchy Process. McGraw- Hill, New York

Sahoo, S. K. and Goswami, S. (2023). A Comprehensive Review of Multiple Criteria Decision-Making (MCDM) Methods: Advancements, Applications, and Future Directions. *Decision Making Advances*, 1, 25-48. https://doi.org/10.31181/dma1120237

Shrestha, A., Mascaro, G., and Garcia, M. (2022). Effects of stormwater infrastructure data completeness and model resolution on urban flood modeling. *Journal of Hydrology*, *607*, 127498. https://doi.org/10.1016/j.jhydrol.2022.127498

Sporleder, B., Fisher, B., Keto, D., Kappel, W., Reddy, J., and DeMott, L. (2021). Methods of data collection and analysis for an assessment of karst aquifer systems between Albany and Buffalo, New York (ver. 2.0, July 2022): *U.S. Geological Survey Scientific Investigations Report*, 2021–5094. https://doi.org/10.3133/sir20215094

Teale, N., and Winter, J. M. (2024). The Relationship between Extreme Precipitation and Damaging Floods in the Northeastern United States. *Journal of Applied Meteorology and Climatology*, 63(9), 1035-1047. https://doi.org/10.1175/JAMC-D-23-0156.1

U.S. Geological Survey Flood Event Viewer (n.d.). U.S. Department of the Interior. https://stn.wim.usgs.gov/fev/

U.S. Geological Survey (2020). 3D Elevation Program 1/3 Arc Second Digital Elevation Model. https://www.usgs.gov/the-national-map-data-delivery

U.S. Geological Survey (2017). Coastal National Elevation Database (CoNED) Topobathymetric Digital Elevation Model. U.S. Geological Survey, Earth Resources Observation and Science (EROS) Center. https://www.usgs.gov/coastal-changes-and-impacts/coned

U.S. Geological Survey (2019). National land cover dataset. U.S. Department of the Interior. https://www.usgs.gov/centers/eros/science/national-land-cover-database

Vozinaki, AE., Karatzas, G., Sibetheros, I., and Varouchakis, E. (2015). An agricultural flash flood loss estimation methodology: the case study of the Koiliaris basin (Greece), February 2003 flood. *Natural Hazards,* 79, 899–920. https://doi.org/10.1007/s11069-015-1882-8

Wang, G., Zhang, X., Zhang, L., and Wang, J. (2019). Application of GIS and the Soil Conservation Service Curve Number method in flood prediction. *Journal of Irrigation and Drainage Engineering*, 145(4), 04019003. https://doi:10.1061/(ASCE)IR.1943-4774.0001425

Wang, X. and Gourbesville, P. (2023). Flash Floods: Forecasting, Monitoring and Mitigation Strategies. *Water*, 15, 1700. https://doi.org/10.3390/w15091700.

Welk, R., Glas, R., Herdman, L., and Fisher, B. (2025). Geospatial datasets of pluvial flood influencing factors used to assess compound flood exposure potential in coastal New York and Connecticut: *U.S. Geological Survey Data Release*. https://doi.org/10.5066/P9N6J1SN

Westenbroek, S., Kelson, V., Dripps, W., Hunt, R., and Bradbury,K. (2010). SWB—A modified Thornthwaite-Mather Soil-Water-Balance code for estimating groundwater recharge: *U.S. Geological Survey Techniques and Methods* 6–A31, 60. https://doi.org/10.3133/tm6A3

White, J., Hunt, R., Fienen, M., and Doherty, J. (2020). Approaches to highly parameterized inversion—PEST++ version 5, a software suite for parameter estimation, uncertainty analysis, management optimization and sensitivity analysis: *U.S. Geological Survey Techniques and Methods*, book 7, chap. C26, 52. https://doi.org/10.3133/tm7C26.

Woolpert (2014). Airborne LiDAR Task Order Report: New York CMGP Sandy 0.7m NPS LiDAR. Prepared for the United States Geological Survey (USGS) under Contract Number G10PC00057, Task Order Number G13PD00797. Woolpert Project Number: 73666. October 2014.

Yilmaz, B. and Harmancioglu, N. (2010). Multi-criteria decision making for water resource management: a case study of the Gediz River Basin, Turkey. Water S.A. 36. 563-576. http://www.wrc.org.za

Supplement

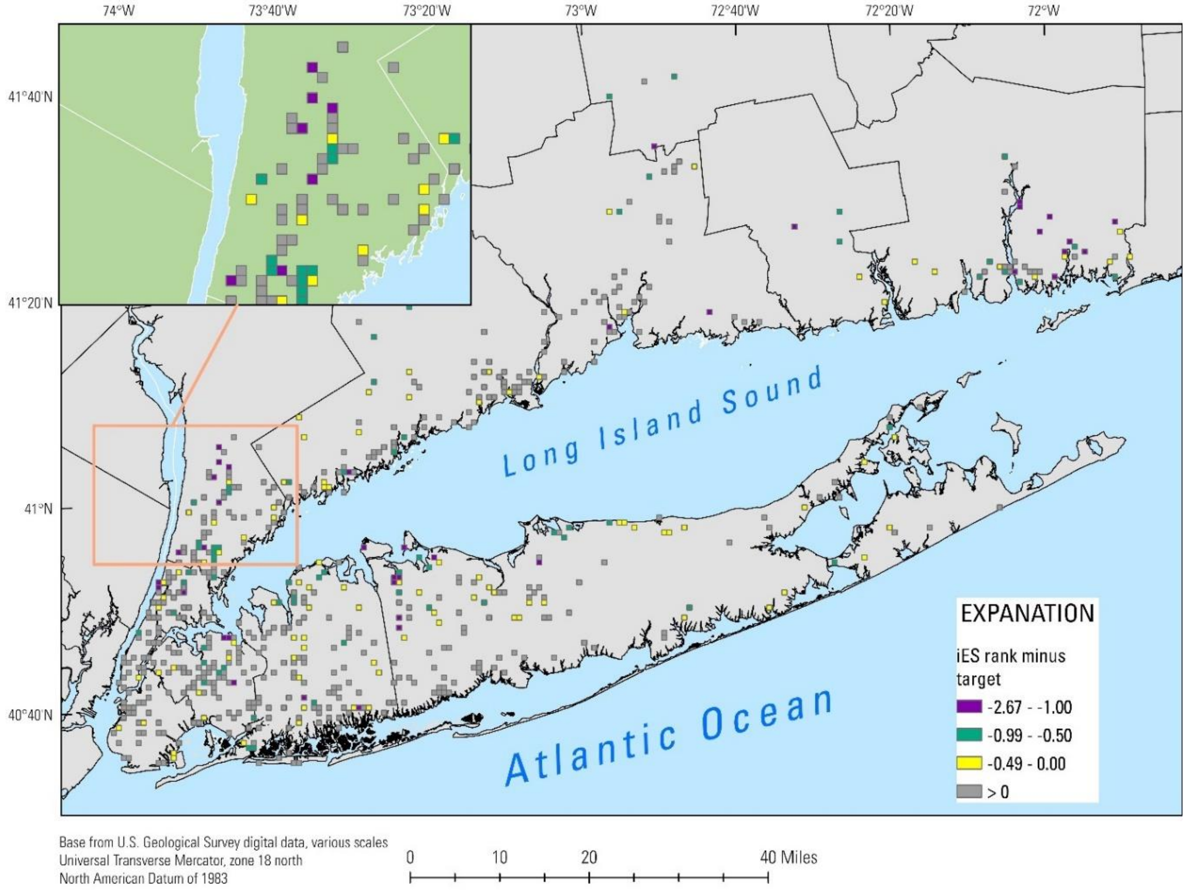

Base from U.S. Geological Survey digital data, various scales
Universal Transverse Mercator, zone 18 north
North American Datum of 1983

Figure S1. Model residuals in each grid cell. Grey cells indicate model target has been met or exceeded.

(a) Drainage Density

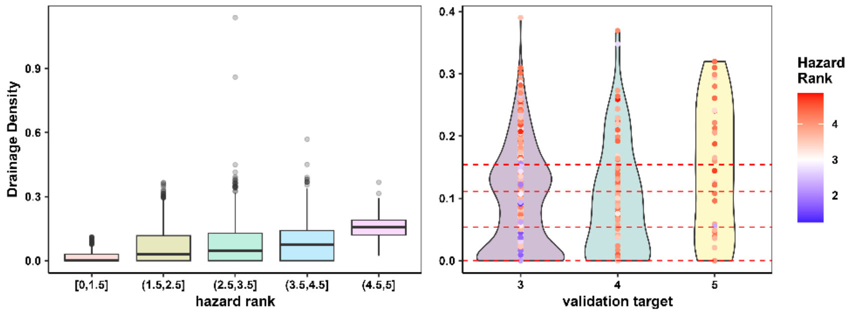

(b) 1-Hour Rainfall

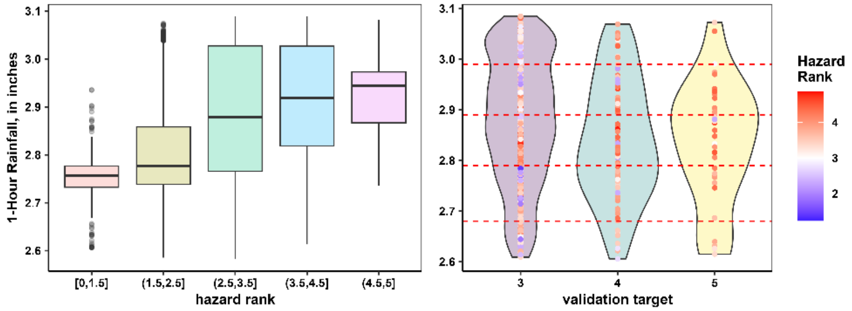

(c) 24-Hour Rainfall

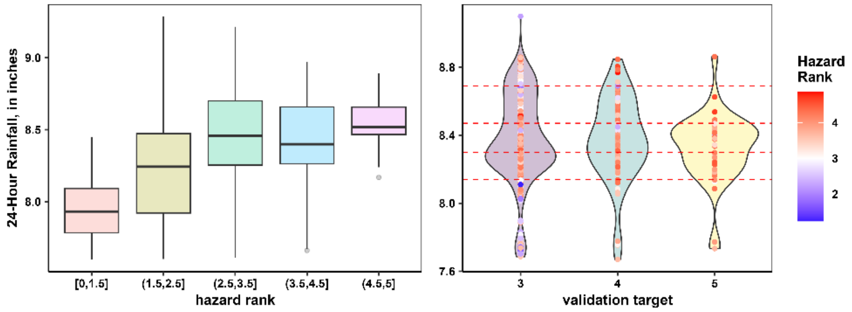

(d) Average Annual Rainfall

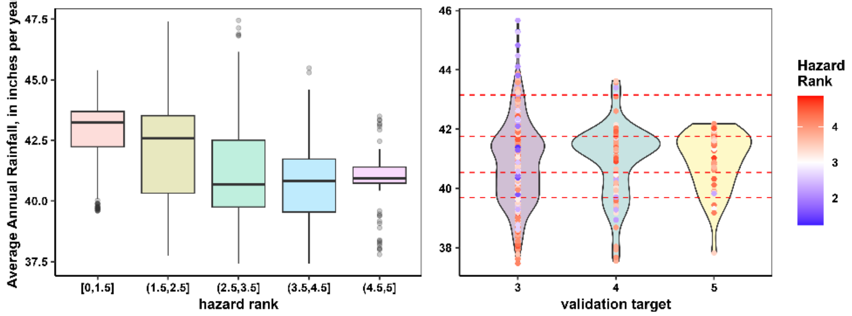

(e) Slope

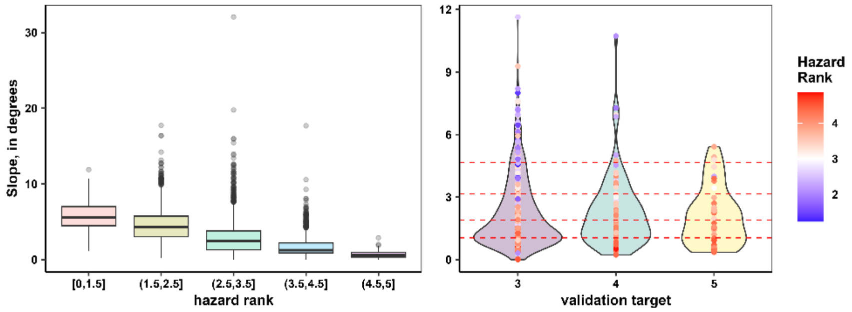

Figure S2a-e. Distributions of flood influencing factors binned by hazard rank (left) and validation target group (right). Each row corresponds to a different factor: (a) drainage density, (b) 1-hour rainfall, (c) 24-hour rainfall, (4) average annual rainfall, and (5) slope. For each row, the left panel shows a boxplot of factor distributions grouped by binned hazard ranks and the right panel shows factor distributions binned by target group, with points representing iES hazard rank. Red dotted lines indicate bin divisions.